MIJST
MIST International Journal of Science and Technology

Next-Gen ECG Technology: Dual Lead System Empowered with IoT Connectivity for Comprehensive Cardiac Monitoring

Samir Fazal Manam, Irfan Ahmed Rifat, Samia Jahan, Md Tobibul Islam*, Md Ushama Shafoyat and Wasil Billah

Department of Biomedical Engineering, Military Institute of Science and Technology, Dhaka, Bangladesh

***Corresponding Email:** *mdtobibulislamthoha@gmail.com*

ARTICLE INFO

Article History:

Received: 13th May 2025
Revised: 05th May 2026
Accepted: 20th May 2026
Published: 30th June 2026

Keywords:
Electrocardiogram (ECG)
Cardiac Monitoring
Healthcare Technology
Internet of Things (IoT)

ABSTRACT

The need for Internet of Things (IoT)- oriented, cost-effective Electrocardiogram (ECG) devices that can remotely measure and transmit ECG signals is becoming increasingly apparent. While standard 12-lead ECG monitoring is effective, its bulky and time-consuming nature poses challenges for remote and continuous monitoring. For developing a cost-effective ECG system, Einthoven's six-lead ECGs are effective but need assessment in real-world conditions. Addressing this gap, this study explores performance evaluation of the dual-lead-to-6-lead ECG monitoring method under 50 Hz noise, electrode reuse, and proximal vs. distal placement. Our system incorporates an ECG circuit that records lead I and lead II data and calculates the 6 leads mathematically. A digital notch filter is applied to the data to enhance signal clarity. The study also includes an arrhythmia-detection component that uses the Pan-Tompkins algorithm to identify abnormal cardiac rhythms promptly. A comprehensive performance analysis of 11 healthy patients was conducted. The reference ECG signals were simultaneously recorded using a BIOPAC MP36 data-acquisition system, with Pearson correlation coefficients ranging from 0.81 to 0.89, with the highest in Lead II. Bland-Altman analysis for R-R interval and Heart rate showed average biases of 11.66 and 0.35, respectively. All data points for both R-R interval and heart rate fell within the ±10% acceptability limits. The proposed technology has potential for telemedicine services and remote patient management, offering an effective solution for continuous, remote ECG monitoring.

1. INTRODUCTION

An electrocardiogram (ECG) is the measurement of the rhythm and electrical activity of the heart. It serves as a vital, non-invasive diagnostic tool for identifying life-threatening cardiovascular diseases (CVDs), including arrhythmias, coronary artery disease, and heart failure. Cardiovascular diseases (CVDs) constitute the foremost global cause of mortality, with an estimated 17.9 million deaths annually, approximately 32% of all global fatalities (Miletic et al., 2024). A large amount of these deaths occur in low-and middle-income countries (LMICs) because timely access to cardiac diagnostics is very limited (Miletic et al., 2024).

Typically, 12-lead ECG signals are used to diagnose cardiac diseases (Yoon & Joo, 2024). It captures electrical activity across both limb leads and precordial leads, enabling the spatial localization of cardiac electrical events such as myocardial infarction or conduction abnormalities (Wang et al., 2024). Since a 12-lead ECG requires 10 electrodes, its application outside the clinical environment is arduous, and precise placement of this requires trained personnel (Miletic et al., 2024).

Recent advances in Internet of Medical Things (IoMT) have increased the need for portable ECG devices (Nguyen & Vo, 2024). The available portable devices on the market generally use single-lead ECG, providing only Lead I (Chen et al., 2024). While single-lead systems are valuable for basic heart rate variability (HRV) analysis, they inherently lack the comprehensive diagnostic depth needed to identify nuanced arrhythmias or ST-segment changes that are crucial for detecting myocardial ischemia, especially in the frontal plane (Chen et al., 2024; Garg et al., 2023). Conversely, 12-lead mobile systems often result in significant motion artifacts and user compliance challenges due to the cumbersome nature of multiple electrodes (Miletic et al., 2024).

So, it is really important to reduce the gap between patient ease of use and diagnostic depth. Subsequently, several studies have attempted to directly reduce the gap between reduced-lead (particularly single-lead) and standard 12-lead ECG systems by reconstructing multi-lead ECG signals from limited lead inputs (Edenbrandt & Pahlm, 1988; Miletic et al., 2024; Nelwan et al., 2004; Seo et al., 2022). Many of these approaches rely on data-driven techniques, such as machine learning and deep learning, to approximate missing leads. For example, advanced architectures such as ensemble learning, residual networks, and attention-based models have been employed to enhance ECG analysis performance (Antoni et al., 2021; Han et al., 2021; Nejedly et al., 2021; Srivastava et al., 2021).

To address these limitations, this study proposes a low-cost dual-lead ECG monitoring system capable of reconstructing six frontal leads (Lead I, II, III, aVR, aVL, and aVF) using deterministic mathematical relationships. The system is integrated within an IoMT-based framework using an ESP32 microcontroller, enabling real-time remote monitoring through both web-based and local graphical user interfaces (GUIs). A digital signal processing pipeline, including a notch filter, is implemented to enhance signal quality, while arrhythmia detection is performed using the Pan–Tompkins algorithm.

The main contributions of this work are as follows (i) development of a cost-effective dual-lead ECG acquisition system with reduced hardware complexity; (ii) mathematical reconstruction of additional ECG leads without the need for data-driven training; (iii) integration of IoMT-based remote monitoring and multi-platform data visualization; and (iv) Implementation of real-time arrhythmia detection for preliminary cardiac assessment.

The proposed system provides an accessible, scalable, and resource-efficient solution for continuous cardiac monitoring, particularly in remote and underserved regions, thereby advancing affordable, connected healthcare technologies.

2. MATERIALS AND METHODS

2.1 Materials Used in Portable ECG Device

The developed ECG signal acquisition system consists of an amplifier circuit, an analogue filter circuit, a 16-bit analogue-to-digital converter, and a microcontroller with a digital notch filter. A communication system was developed using the ESP32. To visualize the ECG signal data, the data were transferred via Wi-Fi to a web interface using the Firebase API. Finally, an enclosure for the device was designed using a 3D printer. Figure 1 depicts the data-acquisition and visualization process for the ECG device. A human subject is connected to a signal-acquisition circuit that captures and filters data. The processed data is then transmitted via an ESP-32 Wi-Fi connection and stored in a NoSQL database. Finally, the data was analysed using Python.

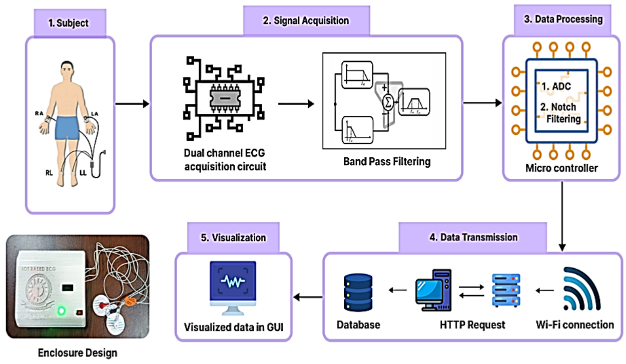

Figure 1: Dual lead ECG acquisition and analysis system.

2.2 Design and Fabrication

Ag/AgCl electrodes are used to acquire the ECG signal from the body. The AD620 instrumentation amplifier was used for its high Common-Mode Rejection Ratio (CMRR) of 100 dB, which is very important for isolating the heart's electrical activity from 50 Hz power-line noise common in domestic environments. As defined in **Eq. (1)**, the gain is set by an external resistor R_G. In our design, the 50 Ω resistor provides a gain of approximately 1000, making it suitable for secondary filtering.

$$R_G = \frac{49.4k\Omega}{G-1} \tag{1}$$

To ensure signal quality, the pre-amplified signal is passed through a multi-stage active filter using the TL074 operational amplifier. This performs in two steps

- Baseline Wander Removal: A high-pass filter with a cutoff of 0.05 Hz removes low-frequency artifacts generally caused by breathing and electrode-skin motion.

- High-Frequency Attenuation: A low-pass filter with a cutoff of 159 Hz removes electronic interference and muscle tremors (electromyographic noise).

We have used TL074 because of its high input impedance and low noise, which ensures the signal remains stable before reaching the microcontroller. The resistors and capacitor values were selected using Eq. (2).

$$F_c = \frac{1}{2\pi RC} \tag{2}$$

The reference voltage was connected to the patient's right leg. Unlike traditional 12-lead machines that rely on a physical Right Leg Driver (RLD) circuit to suppress common-mode voltage, this system achieves a compact form factor by utilizing a 50 Hz IIR Digital Notch Filter within the ESP32 firmware. This allows for the removal of power-line interference in the digital domain, preventing analog component tolerances from affecting filter precision (Wang & Xiao, 2013). Figure 2 shows the implementation circuit for the dual lead system.

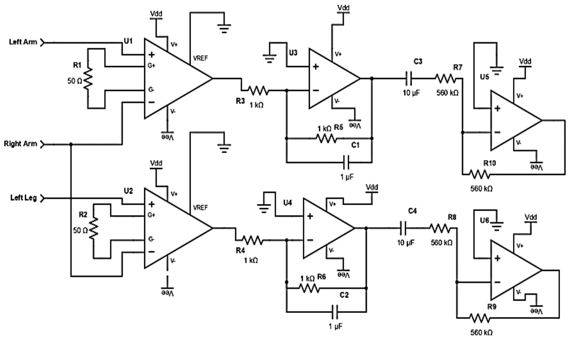

Figure 2: Circuit diagram of a dual-lead ECG monitoring system.

2.3 Lead Conversion

The Lead I and Lead II signals of ECGs were simultaneously converted to digital bits using an external 16-bit analog-to-digital converter. The sample rate was 250 samples per second. The digital bits were calculated to generate an additional 4 leads (lead III, aVR, aVL, and aVF) using the following equations (3-6).

$$\mathrm{LeadIII} = \mathrm{LeadII} - \mathrm{LeadI} \quad (3)$$

$$\mathrm{aVR} = -(\mathrm{LeadI} + \mathrm{LeadII})/2 \quad (4)$$

$$\mathrm{aVL} = (\mathrm{LeadI} - \mathrm{LeadII})/2 \quad (5)$$

$$\mathrm{aVF} = (\mathrm{LeadII} + \mathrm{LeadIII})/2 \quad (6)$$

All ECG leads were then recorded in the cloud database using firebase API for further analysis.

2.4 R-R Intervals and Heart rate detection using Pan Tompkins Method

Arrhythmia detection was achieved using the Pan-Tompkins algorithm (Tueche et al., 2021). The Pan-Tompkins method detects QRS complexes in the ECG waveform. This was achieved through processes such as Bandpass filtering, signal differentiation, squaring, and moving average integration. The algorithm identifies the peaks in the ECG signal corresponding to the QRS complex, which represents ventricular depolarization. The R-R intervals, representing the time between successive QRS complexes, are calculated. Variability in these intervals can indicate irregularities in heart rhythm (CDC, 2024). Based on the R-R intervals, the system classifies the heart rhythm as shown in Figure 3. Deviations from the normal rhythm are flagged as potential arrhythmias. The results are transmitted to the centralized server for further analysis or immediate medical attention if required. The signal processing pipeline consisted of the following stages

Bandpass Filtering

To remove baseline, wander, and high-frequency noise, a bandpass filter was implemented. This filter combines a low-pass and a high-pass filter.

Low-pass filter

The low-pass filter was designed using a 4th-order Butterworth filter with a cutoff frequency of 11 Hz.

$$Nyquist = 0.5 \times Samplerate = 125Hz \quad (7)$$

$$Low = Cutofflow \div Nyquist = \frac{11}{25} = 0.088 \quad (8)$$

High-pass filter

The high-pass filter was designed using a 4th-order

Butterworth filter with a cutoff frequency of 5 Hz.

$$High = Cutoffhigh \div Nyquist = 0.04 \quad (9)$$

The combined bandpass filtering was applied sequentially:

- Low-pass filtering: lowpass_filtered_ecg = lfilter(b_low, a_low, ecg_signal)
- Bandpass filtering: bandpass_filtered_ecg = lfilter(b_high, a_high, lowpass_filtered_ecg)

Derivative Filtering

A derivative filter was applied to enhance the QRS complex. The filter used the following kernel:

$$Derivativefilter = \frac{[-1,-2,0,2,1]}{8} \quad (10)$$

The convolution of the bandpass-filtered ECG signal with the derivative filter was performed as follows: ecg_derivative = np.convolve(badpass_filtered_ecg, derivative_filter, mode ='same'

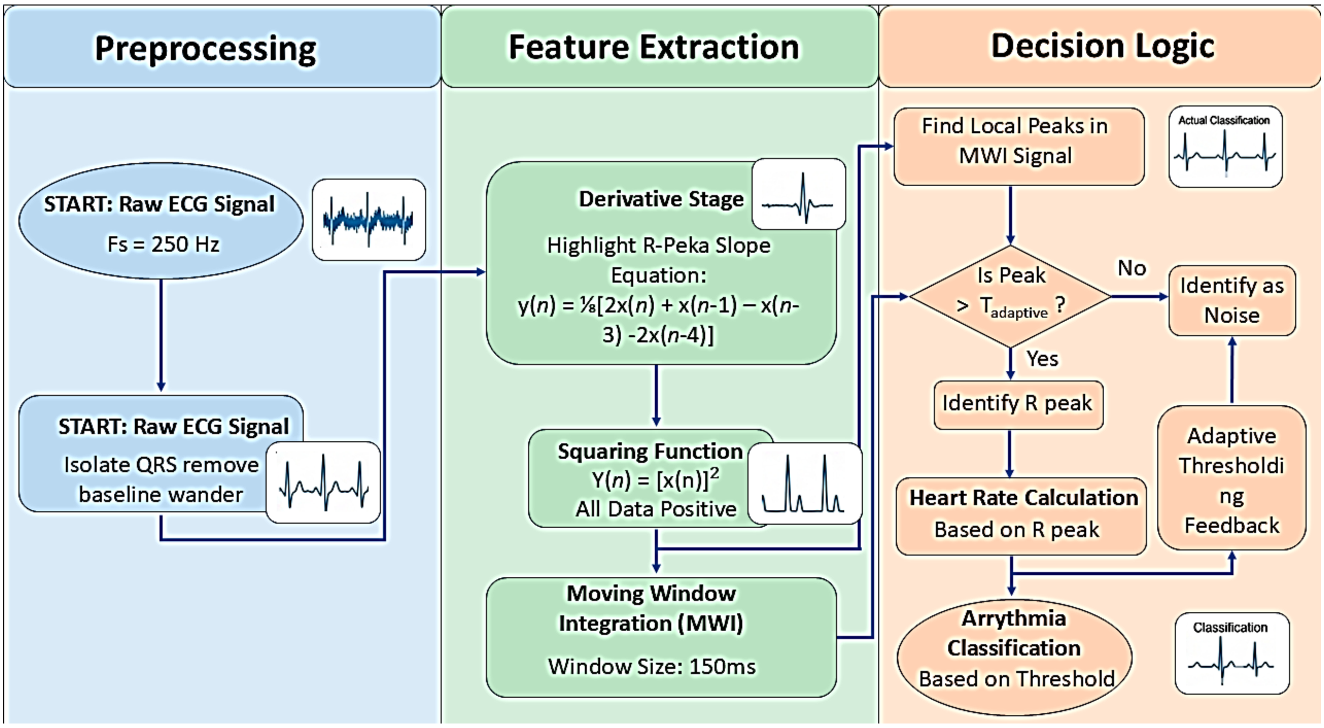

Figure 3: Flowchart of the implemented Pan-Tompkins algorithm for real-time arrhythmia detection.

The process (Figure 3) illustrates the sequential stages of digital signal conditioning, including bandpass filtering and derivative analysis, followed by adaptive thresholding for QRS complex identification and heart rate classification.

Squaring

To amplify the output of the derivative filter, the signal was squared:

$$a.a.eca.a.squared = ecg\_derivative^2 \quad (11)$$

Moving Window Integration

To obtain information on the duration of the QRS complex and to smooth the rectified signal, a moving-window integration was applied. For a sampling frequency (f_s) of 250 Hz, the window size (N) was set to 0.15 seconds based on the typical QRS duration (80–120 ms) (Kurup et al., 2026), corresponding to 37 data points. The integrated signal y(n) is defined by the following discrete convolution (Eq. 12):

$$y(n) = \frac{1}{N}x(n-1) \quad (12)$$

R-peak Detection

R-peaks were detected using the find_peaks function from scipy.signal module with a specified minimum height and distance between peaks:

peak_indices, _ = signal.find_peaks(ecg_integrated, height = 0.0002, distance = sample_rate * 0.6)

RR Interval Calculation

The RR intervals were calculated as the differences between consecutive R-peak indices, converted to seconds:

rr_intervals = np.diff(peak_indices) / sample_rate

Heart Rate Calculation

The heart rate was calculated as the inverse of the mean RR interval, converted to beats per minute (bpm):

heart_rate = 60 / np.mean(rr_intervals)

Arrhythmia Classification

Based on the calculated heart rate, arrhythmias were classified as follows (Tachycardia vs. Bradycardia):

- Normal heart rate: 60-100 bpm
- Bradycardia: < 60 bpm
- Tachycardia: > 100 bpm

By applying these criteria, the heart rhythms were classified into the appropriate categories, aiding in the detection and analysis of arrhythmias.

2.5 Quantitative Evaluation

Quantitative assessment of the derived six limb leads was performed by direct comparison with simultaneously acquired standard limb leads. The reference ECG signals were simultaneously recorded using a BIOPAC MP36 data acquisition system (BIOPAC Systems Inc., Goleta, CA, USA). The MP36 is a 4-channel physiological measurement unit commonly used in biomedical education and research. ECG signals were acquired using ECG100C amplifier modules at a sampling frequency of 1000 Hz and a bandpass filter setting of 0.05–150 Hz, in accordance with standard electrocardiography guidelines. Signals were collected simultaneously from both devices. The start point was selected from the first R peak of the ECG to ensure proper signal alignment. All analyses were conducted using data collected from the 11 healthy volunteers under the various real-world conditions described previously (electrode placement, reuse cycles, and 50 Hz noise levels). Raw ECG signals from both the proposed dual-lead system and the reference medical-grade device were pre-processed using identical procedures to ensure fair comparison. Signals were resampled to 250 Hz when necessary. R-peak detection was performed using the Pan-Tompkins algorithm, and representative beats were obtained by averaging 10–20 aligned cardiac cycles per recording segment. The following quantitative metrics (Eq. 13, 14, and 15) were computed for each of the six limb leads separately and as an overall average:

Pearson correlation coefficient (r): Measures the linear similarity in waveform morphology between the derived and direct leads, defined as:

$$Pearson\ Correlation\ Coefficient = \left\{ \frac{\sum_{i=1}^{N} \hat{y}[i] * y[i]}{\left(\sum_{i=1}^{N} y[i]^2 * \sum_{i=1}^{N} \hat{y}[i]^2\right)^{\frac{1}{2}}} \right\} \tag{13}$$

Root Mean Square Error (RMSE): Calculated in microvolts (µV) to quantify absolute amplitude differences.

$$RMSE = \sqrt{\frac{\sum_{i=1}^{N} (y|i| - \hat{y}\ |i|)^2}{N}} \tag{14}$$

Percentage Root Mean Square Difference (PRD):

$$PRD = \frac{\sqrt{\frac{1}{N}\sum_{i=1}^{N}(xi-xj)^{\wedge}2}}{RMS_{signal}} \times 100\% \tag{15}$$

Normalized error measure expressed as a percentage.

Where N is the length of the ECG segments in samples, y is the actual measured ECG, and x is the derived ECG. These metrics were calculated both on the entire 10-second waveform and on averaged representative beats.

2.6 Enclosure Design

An enclosure was developed using Computer-Aided Design (CAD) software, particularly SolidWorks (SD), as shown in Figure 4. The overall dimensions of the enclosure are 186 mm x 175 mm x 70 mm.

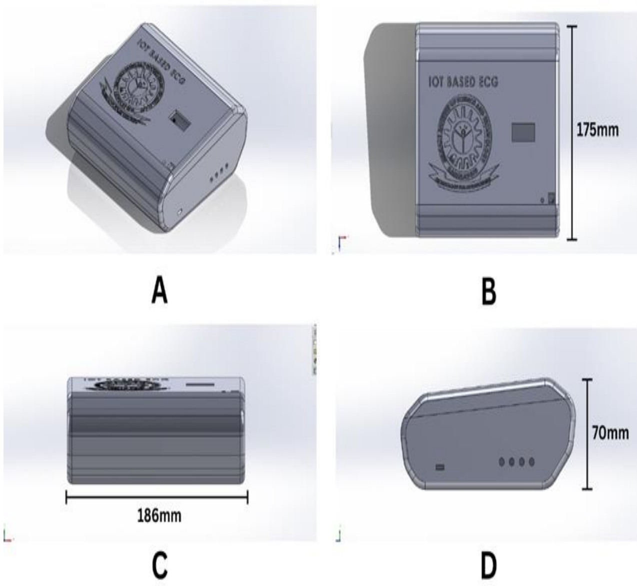

Figure 4: CAD design of the portable enclosure showing (A) isometric, (B) top, (C) front, and (D) side views.

3. RESULTS AND DISCUSSIONS

A total of 11 healthy volunteers (6 males, 5 females, range 25–35 years) with no history of cardiac disease participated in the study. For each participant, simultaneous ECG recordings were obtained across all combinations of electrode placement (distal limb vs. proximal/torso), electrode reuse cycles (0-3), and noise conditions (clean vs. controlled 50 Hz interference at low, moderate, and high levels). A minimum of three 10-second segments were recorded per condition for quantitative comparison between mathematically derived six limb leads and directly recorded reference leads from BIOPAC MP36. Figure 5 shows the ECG lead comparison for a patient.

3.1 Overall Waveform Similarity between Derived and Direct Leads

The findings show moderate to good wave-shape correlation for leads I, II, and aVR, with Pearson correlation coefficients of 0.81-0.89. The lead with the highest correlation is lead II (clinically significant), with an r-value of 0.8864. Nevertheless, leads III and aVL had relatively poor correlation with respective values of 0.3446 and 0.5644. This is due to the mathematical limitations of Einthoven's triangle-based reconstruction when input signals contain noise or minor placement variations. Also, the small gain mismatch between the reference device and the developed device can distort the signal. Lead III is very sensitive to amplitude mismatch. The values of the PRD were quite high for all the leads (106% – 150%), indicating that even though some aspects of the morphological pattern had been retained, there was considerable discrepancy in the amplitude and shape of the ECG in the synthesized leads compared to those obtained directly. The results of the mean Pearson correlation coefficient (r), Root Mean Square Error (RMSE), and Percentage Root Mean Square Difference (PRD) are listed in Table 1 for all 11 subjects.

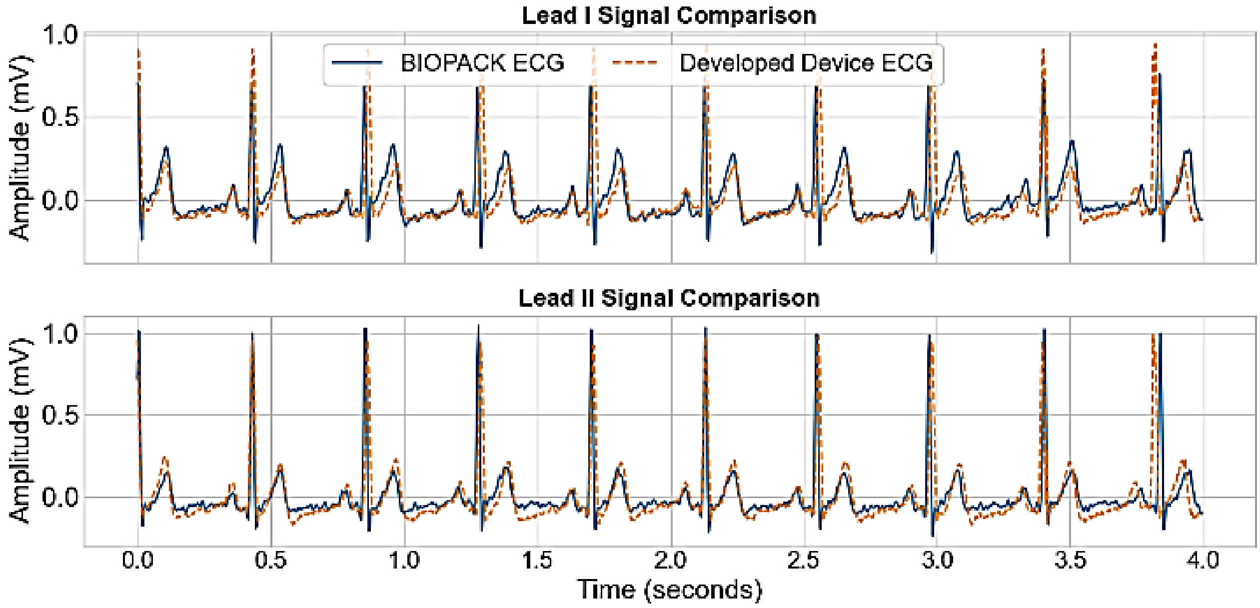

Figure 5: Lead I and Lead II ECG Signals overlap from the developed device and BIOPACK MP36.

Table 1: Overall performance metrics of derived versus direct limb leads (n = 11 subjects)

Lead	Pearson r	RMSE (µV)	PRD (%)
I	0.8056	0.1393	106.11
II	0.8864	0.1307	116.21
III	-0.0344	0.0835	125.79
aVF	0.7483	0.0861	149.89
aVL	0.5644	0.0940	109.96
aVR	0.8725	0.1281	107.47
Overall (6 leads)	0.6388	0.1103	119.24

3.2 Effect of 50 Hz Power-Line Noise

The performance of the digital notch filter degraded progressively as the level of 50 Hz interference increased. Table 2 presents the mean Pearson correlation coefficient across all six limb leads under different noise conditions.

The results demonstrate a clear negative impact of power-line interference on reconstruction accuracy. Moderate levels of 50 Hz noise resulted in a statistically significant decrease in waveform similarity. The correlation decreased to 0.49 at high noise levels (1.0 mV), indicating poor lead quality due to significant degradation. While the digital notch filter performed well in typical household conditions,

Table 2: Influence of 50 Hz noise on derivation accuracy (mean Pearson r ± SD across 6 leads, n = 11)

Noise Condition	Mean Pearson	RMSE (µV)	p-value
Clean (baseline)	0.72 ± 0.08	0.098	-
Low 50 Hz (0.1 mV)	0.65 ± 0.11	0.112	0.032
Moderate 50 Hz (0.5 mV)	0.58 ± 0.14	0.125	0.004
High 50 Hz (1.0 mV)	0.49 ± 0.17	0.141	< 0.001

it was inadequate under strong interference. Thus, it is suggested that analog preprocessing and appropriate shielding be considered in subsequent work to ensure the noise resistance of ECG devices in real-life applications.

3.3 Impact of Electrode Reuse and Placement

The reusability of the electrodes and their positioning affected the accuracy of the leads acquired. The values of the mean Pearson correlation coefficient (with respect to six limb leads) for two electrode reuse cycles in two locations are provided in Table 3.

Table 3: Effect of electrode reuse cycles and placement on derivation performance (mean Pearson r ± SD, n = 11)

Reuse Cycles	Distal Placement (Standard)	Proximal Placement (Closer to Heart)	p-value (Distal vs Proximal)
0 times (New)	0.71 ± 0.09	0.68 ± 0.10	0.21
1 time	0.67 ± 0.11	0.63 ± 0.12	0.09
2 times	0.61 ± 0.13	0.57 ± 0.15	0.04
3 times	0.52 ± 0.16	0.48 ± 0.18	0.03

Further reuse of electrodes beyond 2 cycles reduced the accuracy of the derivation, regardless of the electrode placement type. The proximal placement of electrodes yielded somewhat lower correlation coefficients compared to distal placement. There were significant differences between the two groups after the 2nd and 3rd reuse cycles, with p-values of 0.04 and 0.03, respectively.

3.4 Agreement on Diagnostic Parameters (Bland-Altman Analysis)

The Bland-Altman analysis was conducted to compare the diagnostic parameters between the derived limb leads and the reference direct leads acquired using the BIOPAC MP36 system. The analysis focused on two key diagnostic parameters: R-R interval and heart rate. Table 4 shows the Bias, 95% limits of agreement, and the percentage of points within 10% for the R-R interval and Heart Rate derived from the Pan Tomkinson algorithm.

Table 4: R-R interval and Heart Rate

Parameter	Bias (ms)	95% Limits of Agreement (ms)	% of points within ±10%
R-R Interval	11.66	-9.22 to 32.53	100.00%
Heart Rate	0.35	-1.63 to 2.32	100.00%

According to the results, there is a good clinical agreement between the two leads. The entire range of measurements for both R-R interval and heart rate falls within ±10% of the acceptable range. The Bias for R-R interval is 11.66 ms with relatively tight 95% limits of agreement, implying a small degree of systematic error. On the other hand, the Bias for heart rate is 0.35 bpm, indicating excellent correlation between the results obtained using the two methods. This shows that, even though there are moderate levels of waveform reconstruction error in some leads, the derived waveforms are accurate enough for diagnostic purposes, such as measuring heart rate and R-R intervals. Figure 6 displays the Bland-Altman plot for the RR interval. The x-axis represents the mean of the two methods, while the y-axis shows the difference.

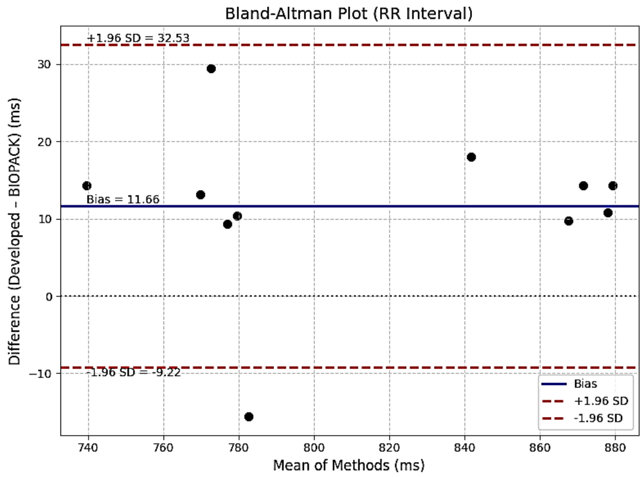

Figure 6: Bland–Altman plot showing agreement between the BIOPACK reference system and the developed device for RR interval measurements.

4. CONCLUSIONS

In this paper, we developed the hardware and software for a low-cost dual-lead ECG device. We used low-power components to make the system portable, including rechargeable lithium-ion batteries, instrumentation amplifiers, and disposable electrodes. Although 12-lead ECG devices are available in hospitals, they are not as affordable as household devices, continuous monitoring equipment, or primary screening equipment. We removed most of the complex circuitry by using code, such as using a digital notch filter and mathematically calculating an additional 4 leads. In this study, we also developed several GUIs to visualize the data. The GUI app developed in Python can be run as a Windows app. The websites are responsive and can store all the incoming data. This work could also be extended to build a more integrated hardware system, such as a large display screen to visualize the data, with the GUI embedded. Also, an encryption and security system on the website could be implemented. This word can help develop low-cost ECG monitoring devices with remote sharing, thereby saving time and improving healthcare quality.

ACKNOWLEDGMENTS

The authors want to express our sincere gratitude to the head of the Department of Biomedical Engineering (BME) and the Centre for Army Research and Development (CARD) for their invaluable support in developing this IoT-based ECG machine. We are deeply grateful to the CARD for their generous financial support, which was pivotal in the development of this IoT-based ECG machine.

DATA AVAILABILITY STATEMENT

Datasets generated during the current study are available from the corresponding author upon reasonable request.

FUNDING DECLARATION

This research was financially supported by the Centre for Army Research and Development (CARD).

ETHICS APPROVAL

This study is an engineering experimental investigation. The MIJST Research Ethics Committee has confirmed that formal ethical approval was not required.

ETHICS, CONSENT TO PARTICIPATE, AND CONSENT TO PUBLISH

Not applicable.

COMPETING INTERESTS

The authors declare that they have no competing interests.

AUTHOR CONTRIBUTIONS

Author 1: conceptualisation, methodology development, data collection, and preparation of the initial manuscript draft.
Author 2: Data analysis, literature review, result interpretation, and manuscript writing.
Author 3: Data organisation, validation, visualisation, and critical revision of the manuscript.
Author 4: Conceptualisation, methodology refinement, manuscript review, editing, and handling correspondence related to the manuscript.
Author 5: Formal analysis, technical review, and improvement of the manuscript structure.
Author 6: Wasil Billah - literature review, formatting, referencing, and manuscript draft.

ARTIFICIAL INTELLIGENCE ASSISTANCE STATEMENT

No AI tools were used. The authors take full responsibility for the accuracy and integrity of the manuscript.

CONFLICT OF INTEREST DECLARATION

The authors declare that they have no conflicts of interest.

REFERENCES

Antoni, L., Bruoth, E., Bugata, P., Gajdos, D., Horvat, S., Hudak, D., Kmecova, V., Stana, R., Stankova, M., Szabari, A., & Vozarikova, G. (2021). A two-phase multilabel ECG classification using a one-dimensional convolutional neural network and modified labels. *Computing in Cardiology*. https://doi.org/10.23919/CINC53138.2021.9662878

Chen, J., Wu, W., Liu, T., & Hong, S. (2024). Multi-channel masked autoencoder and comprehensive evaluations for reconstructing 12-lead ECG from an arbitrary single-lead ECG. *npj Cardiovascular Health*, *1*(1), Article 34. https://doi.org/10.1038/s44325-024-00036-4

Edenbrandt, L., & Pahlm, O. (1988). Vectorcardiogram synthesized from a 12-lead ECG: Superiority of the inverse Dower matrix. *Journal of Electrocardiology*, *21*(4), 361–367. https://doi.org/10.1016/0022-0736(88)90113-6

Garg, A., Venkataramani, V. V., & Priyakumar, U. D. (2023). Single-lead to multi-lead electrocardiogram reconstruction using a modified attention U-Net framework. *Proceedings of the International Joint Conference on Neural Networks*. https://doi.org/10.1109/IJCNN54540.2023.10191213

Han, H., Park, S., Min, S., Choi, H. S., Kim, E., Kim, H., Park, S., Kim, J., Park, J., An, J., Lee, K., Jeong, W., Chon, S., Ha, K., Han, M., & Yoon, S. (2021). Towards high generalization performance on electrocardiogram classification. *Computing in Cardiology*. https://doi.org/10.23919/CINC53138.2021.9662737

Kurup, A. R., Kar, M. K., Mishra, M., Dev, S., & Neog, D. R. (2026). Transformer-based generative adversarial network with multi-scale temporal attention for ECG synthesis and PQRST feature preservation. *IEEE Access*, *1–1*. https://doi.org/10.1109/ACCESS.2026.3656370

Miletic, M. N., Atanasoski, V. A., Belicev, P. P., Gligoric, G. M., Ralevic, U. M., Krsic, J. B., Obradovic, A. D., Lazovic, A., Stojanovic, D. B., Petrovic, J., Babic, R., Vukajlovic, D., Hadzievski, L. R., Bojovic, B. P., Panescu, D., & Vajdic, B. (2024). Accurate reconstruction of the 12-lead electrocardiogram from a 3-lead electrocardiogram measured by a mobile device. *IEEE Access*, *12*, 79765–79775. https://doi.org/10.1109/ACCESS.2024.3408412

Nejedly, P., Ivora, A., Smisek, R., Viscor, I., Koscova, Z., Jurak, P., & Plesinger, F. (2021). Classification of ECG using ensemble of residual CNNs with attention mechanism. *Computing in Cardiology*. https://doi.org/10.23919/CINC53138.2021.9662723

Nelwan, S. P., Kors, J. A., Meij, S. H., Van Bemmel, J. H., & Simoons, M. L. (2004). Reconstruction of the 12-lead electrocardiogram from reduced lead sets. *Journal of Electrocardiology*, *37*(1), 11–18. https://doi.org/10.1016/J.JELECTROCARD.2003.10.004

Nguyen, H. H., & Vo, T. T. (2024). Enhancing cardiovascular health monitoring through IoT and deep learning technologies. *SN Computer Science*, *5*(5), Article 608. https://doi.org/10.1007/S42979-024-02962-7

Seo, H. C., Yoon, G. W., Joo, S., & Nam, G. B. (2022). Multiple electrocardiogram generator with single-lead electrocardiogram. *Computer Methods and Programs in Biomedicine*, *221*, Article 106858. https://doi.org/10.1016/J.CMPB.2022.106858

Srivastava, A., Hari, A., Pratiher, S., Alam, S., Ghosh, N., Banerjee, N., & Patra, A. (2021). Channel self-attention deep learning framework for multi-cardiac abnormality diagnosis from varied-lead ECG signals. *Computing in Cardiology*. https://doi.org/10.23919/CINC53138.2021.9662886

Wang, L. H., Zou, Y. Y., Xie, C. X., Yang, T., & Abu, P. A. R. (2024). Feasibility and validity of using deep learning to reconstruct 12-lead ECG from three-lead signals. *Journal of Electrocardiology*, *84*, 27–31. https://doi.org/10.1016/J.JELECTROCARD.2024.03.004

Yoon, G. W., & Joo, S. (2024). Classification feasibility test on multi-lead electrocardiography signals generated from single-lead electrocardiography signals. *Scientific Reports*, *14*(1), Article 1888. https://doi.org/10.1038/s41598-024-52216-y

Antoni, L., Bruoth, E., Bugata, P., Gajdos, D., Horvat, S., Hudak, D., Kmecova, V., Stana, R., Stankova, M., Szabari, A., & Vozarikova, G. (2021). A Two-Phase

Multilabel ECG Classification Using One-Dimensional Convolutional Neural Network and Modified Labels. Computing in Cardiology. https://doi.org/10.23919/CINC53138.2021.9662878

Chen, J., Wu, W., Liu, T., & Hong, S. (2024). Multi-channel masked autoencoder and comprehensive evaluations for reconstructing 12-lead ECG from an arbitrary single-lead ECG. Npj Cardiovascular Health, 1:1, 1(1), 34-. https://doi.org/10.1038/s44325-024-00036-4

Edenbrandt, L., & Pahlm, O. (1988). Vectorcardiogram synthesized from a 12-lead ECG: Superiority of the inverse Dower matrix. Journal of Electrocardiology, 21(4), 361–367. https://doi.org/10.1016/0022-0736(88)90113-6

Garg, A., Venkataramani, V. V., & Priyakumar, U. D. (2023). Single-Lead to Multi-Lead Electrocardiogram Reconstruction Using a Modified Attention U-Net Framework. Proceedings of the International Joint Conference on Neural Networks. https://doi.org/10.1109/IJCNN54540.2023.10191213

Han, H., Park, S., Min, S., Choi, H. S., Kim, E., Kim, H., Park, S., Kim, J., Park, J., An, J., Lee, K., Jeong, W., Chon, S., Ha, K., Han, M., & Yoon, S. (2021). Towards High Generalization Performance on Electrocardiogram Classification. Computing in Cardiology, https://doi.org/10.23919/CINC53138.2021.9662737

Kurup, A. R., Kar, M. K., Mishra, M., Dev, S., & Neog, D. R. (2026). Transformer-based Generative Adversarial Network with Multi-Scale Temporal Attention for ECG Synthesis and PQRST Feature Preservation. IEEE Access, 1–1. https://doi.org/10.1109/ACCESS.2026.3656370

Miletic, M. N., Atanasoski, V. A., Belicev, P. P., Gligoric, G. M., Ralevic, U. M., Krsic, J. B., Obradovic, A. D., Lazovic, A., Stojanovic, D. B., Petrovic, J., Babic, R., Vukajlovic, D., Hadzievski, L. R., Bojovic, B. P., Panescu, D., & Vajdic, B. (2024). Accurate Reconstruction of the 12-Lead Electrocardiogram From a 3-Lead Electrocardiogram Measured by a Mobile Device. IEEE Access, 12, 79765–79775. https://doi.org/10.1109/ACCESS.2024.3408412

Nejedly, P., Ivora, A., Smisek, R., Viscor, I., Koscova, Z., Jurak, P., & Plesinger, F. (2021). Classification of ECG Using Ensemble of Residual CNNs with Attention Mechanism. Computing in Cardiology. https://doi.org/10.23919/CINC53138.2021.9662723

Nelwan, S. P., Kors, J. A., Meij, S. H., Van Bemmel, J. H., & Simoons, M. L. (2004). Reconstruction of the 12-lead electrocardiogram from reduced lead sets. Journal of Electrocardiology, 37(1), 11–18. https://doi.org/10.1016/J.JELECTROCARD.2003.10.004

Nguyen, H. H., & Vo, T.T. (2024). Enhancing Cardiovascular Health Monitoring Through IoT and Deep Learning Technologies. SN Computer Science, 5:5, 5(5), 608-. https://doi.org/10.1007/S42979-024-02962-7

Seo, H. C., Yoon, G. W., Joo, S., & Nam, G. B. (2022). Multiple electrocardiogram generator with single-lead electrocardiogram. Computer Methods and Programs in Biomedicine, 221, 106858. https://doi.org/10.1016/J.CMPB.2022.106858

Srivastava, A., Hari, A., Pratiher, S., Alam, S., Ghosh, N., Banerjee, N., & Patra, A. (2021). Channel Self-Attention Deep Learning Framework for Multi-Cardiac Abnormality Diagnosis from Varied-Lead ECG Signals. Computing in Cardiology. https://doi.org/10.23919/CINC53138.2021.9662886

Wang, L. H., Zou, Y. Y., Xie, C. X., Yang, T., & Abu, P. A. R. (2024). Feasibility and validity of using deep learning to reconstruct 12-lead ECG from three-lead signals. Journal of Electrocardiology, 84, 27–31. https://doi.org/10.1016/J.JELECTROCARD.2024.03.004

Yoon, G. W., & Joo, S. (2024). Classification feasibility test on multi-lead electrocardiography signals generated from single-lead electrocardiography signals. Scientific Reports 2024 14:1, 14(1), 1888-. https://doi.org/10.1038/s41598-024-52216-y